coatings

MDPI

Article

Recovery Behavior of Microstructured Thiol-Ene Shape-Memory Film

Algirdas Lazauskas *, Viktoras Grigaliūnas and Dalius Jucius

Institute of Materials Science, Kaunas University of Technology, K. Baršausko 59, LT51423 Kaunas, Lithuania; viktoras.grigaliunas@ktu.lt (V.G.); dalius.jucius@ktu.lt (D.J.)

* Correspondence: algirdas.lazauskas@ktu.edu; Tel.: +370-671-73375

Received: 14 March 2019; Accepted: 17 April 2019; Published: 20 April 2019

Abstract: In this work, surface microstructurization was coupled with shape-memory polymer to generate reversibly tunable surface properties. A photopolymerizable thiol-ene composition comprising a mixture of pentaerythritol tetrakis(3-mercaptopropionate) (PETMP), 1,3,5-triallyl-1,3,5-triazine-2,4,6(1H,3H,5H)-trione (TTT) and 2,2-dimethoxy-2-phenylacetophenone (DMPA) was used to prepare microstructured thiol-ene shape-memory film via casting and UV polymerization on the electron beam lithography fabricated arrays of 1 μm and 2 μm square pits. The mechanical deformation via compression and recovery of the surface microstructure were investigated. Results show that, after heat treatment of the deformed thiol-ene film, the recovery yields for microstructures were not worse than 90% ± 2% and 93% ± 2% for structures imprinted with 1 μm and 2 μm square pit micro imprint stamps. Additionally, heat treatment of deformed thiol-ene film resulted in the recovery of intense diffraction colors and laser diffraction patterns. This study opens up an avenue of incorporating microstructured shape-memory films for new products, e.g., optical security devices, superhydrophobic coatings, medical diagnostics and biosensors.

Keywords: photopolymerizable; thiol-ene network; microstructured film; mechanical deformation; recovery; shape-memory

1. Introduction

Shape-memory polymers (SMPs) belong to the class of smart materials. They can remember their permanent shape and return to it from a deformed temporary shape under an external stimulus such as heat, light, microwaves, pressure, pH, moisture, solvent, electric and magnetic fields [1,2]. In recent years, SMPs have gained significant interest for fundamental research and applications in medicine, photonics, smart textiles, microelectromechanical systems, aerospace, etc. [3]. As a rule, such polymers exhibit special molecular structures consisting of two kinds of segments: stable netpoints, formed by interpenetrating networks, crystalline regions or chemical crosslinks, and reversible segments [4]. The netpoints are responsible for recovery of the permanent shape, whereas reversible segments serve to fix the temporary shape by crystallization, glass transition or reversible bonds. So far, heat is the most common external stimulus used to trigger shape recovery above the activation temperature of SMP. Activation of the material can take place at the glass transition or the melting temperature as well as at the temperature at which reversible intermolecular bonds can be broken [5]. Latest trends in the design of novel SMPs involve noncovalent supramolecular interactions [6], shape-memory polymer composites [7], multishape, reversible and multifunctional SMPs [4,8] and the development of new shape-memory thermosets [9].

Recently, a number of studies related to the microstructuring, deformation and recovery of SMPs have been conducted, as this could bring the possibility of controlling the surface properties for a wide range of applications including the manipulation of wettability as well as the light diffraction and

optical parameters. For instance, the effects of geometry and size on the deformation and recovery of the imprinted surface texture in a shape-memory thermoplastic elastomer polyetherurethane were systematically investigated in [10]. Micro-sized protrusion arrays in thermo-responsive shape-memory polystyrene have been produced using laser heating and indentation processes, and it has been shown that indentation is a more convenient approach than laser heating [11]. The relaxation of very narrow polystyrene gratings fabricated by nanoimprint lithography was studied in [12]. It was shown that surface wettability for flow regulation can be controlled using high-aspect-ratio microstructures fabricated in epoxy-based shape-memory polymers [13] or liquid crystalline elastomers [14]. Shape-memory elastomer has been demonstrated as an effective material for shape-memorizing micro-optics—the surface microstructures including shape-memory holograms can be erased by compression and then can be quickly restored to their original condition by heating [15].

Thiol-ene polymers are attractive thermosets with shape-memory properties. Thiol-ene polymerizations occur rapidly via radical-mediated step-growth reaction with a low volume shrinkage, and they are insensitive to molecular oxygen and water, yielding a uniform crosslinked polymer network exhibiting toughness, flexibility, improved adhesion and high optical transparency [16–18]. Thiol–ene polymerization with mercaptopropionate thiol monomers proceeds faster compared to mercaptoacetate or aliphatic thiol monomers due to its ability to form a six-membered ring through hydrogen bonding, which stabilizes thiyl radicals [19,20]. Ene monomers with high electron density are commonly desired as they exhibit rapid rates of thiol–ene polymerization. The polymerization reaction is initiated via the use of photoinitiators, e.g., direct cleavage initiators such as 2,2-dimethoxy-2-phenylacetophenone and the excitation of diaryl ketones followed by hydrogen abstraction [21,22]. Radical termination occurs via bimolecular radical–radical recombination [23]. Moreover, crosslinked thiol-ene polymers exhibit excellent chemical resistance for different types of aliphatic and aromatic solvents and are stable in harsh conditions, such as temperatures from −150 to 125 °C [24]. White et al. examined the performance of holographic polymer dispersed liquid crystals made from thiol-ene polymerizations with a particular focus on fast-reacting systems containing triallyl isocyanurate [25]. These liquid crystals were shown to be very promising materials with switchable diffractive capabilities. In 2010, Nair et al. first described the use of thiol-ene photopolymers as shape-memory polymer systems exhibiting excellent shape fixity and distinct shape-memory actuation response [17]. Recently, our group designed a thiol-ene shape-memory-assisted scratch-healing polymer system that not only responds to the temperature changes as the external stimulus, but is also capable of initiating scratch recovery at ambient temperature conditions [26].

In this work, microstructured shape-memory thiol-ene films were fabricated using a casting and UV polymerization technique on the textured silicon substrates. The mechanical deformation via compression and recovery of the surface microstructure were investigated by employing optical and atomic force microscopy. In addition, laser diffraction patterns were shown to be suitable for the rapid evaluation of recovered shape-memory profiles. To our knowlegde, the recovery behavior of microstructures fabricated in shape-memory thiol-ene film was investigated here for the first time.

2. Materials and Methods

2.1. Materials

All reagents and solvents were obtained at the highest purity and used without further purification unless otherwise specified. For instance, 1,3,5-triallyl-1,3,5-triazine-2,4,6(1H,3H,5H)-trione (TTT, trifunctional allyl component), pentaerythritol tetrakis(3-mercaptopropionate) (PETMP, tetrafunctional thiol component), 2,2-dimethoxy-2-phenylacetophenone (DMPA, photoinitiator), isopropyl alcohol (IPA), acetone and methyl isobutyl ketone (MIBK) were obtained from Sigma-Aldrich (St. Louis, MO, USA). The poly(methyl methacrylate) (PMMA) 4% solution in anisole with a molecular weight of 950 K and conductive polymer L1_XP were obtained from Micro Resist Technology (Berlin, Germany).

Double side polished silicon (100) wafers with a thickness of 500 ± 20 μm were obtained from University Wafer (Boston, MA, USA).

2.2. Fabrication of the Micro Imprint Stamp

The micro imprint stamp was fabricated by combining electron beam lithography and reactive ion etching techniques. A Raith e-LiNEplus electron beam lithography system (Dortmund, Germany) was used to pattern the test microstructures on a silicon substrate in the form of two arrays of 1 and 2 μm square pits with periods of 2 and 4 μm, respectively (the periods were identical in both directions; the patterning area size for every array was 6×6 mm^2). The silicon substrates were cleaned in solvents (IPA, acetone) and then dried with a nitrogen flow. The PMMA 4% solution in anisole with a molecular weight of 950 K was spin coated on silicon substrates at 3000 rpm for 40 s and dried for 5 min at 180 °C on a hotplate (the targeted film thickness was achieved to be about 220 nm). Then a layer of conductive polymer L1_XP was spin coated at 3000 rpm and dried for 2 min at 80 °C on a hotplate. Electron beam patterning was conducted with an acceleration voltage of 10 kV (aperture size: 60 μm; write field size: 1000×1000 μm^2; beam current: 1263 pA). The exposure dose was kept constant at 120 μC/cm^2. The exposed PMMA resist was developed at 18 °C in a 1:3 MIBK and IPA mixture for 30 s. Development was stopped in IPA and the substrates were dried with a nitrogen gas flow. A Raith e-LiNEplus scanning electron microscope (SEM) was used to observe the fabricated test microstructures (Figure 1). Reactive ion etching of silicon was conducted in a radio frequency (RF) asymmetric diode system PK-2420RIE (Plasma-Therm Inc., Saint Petersburg, FL, USA) via the use of SF_6 plasma chemistry. Etching conditions are presented in Table 1. The fabricated micro imprint stamps with square pit periods of 2 and 4 μm were denoted as 2A and 4B, respectively.

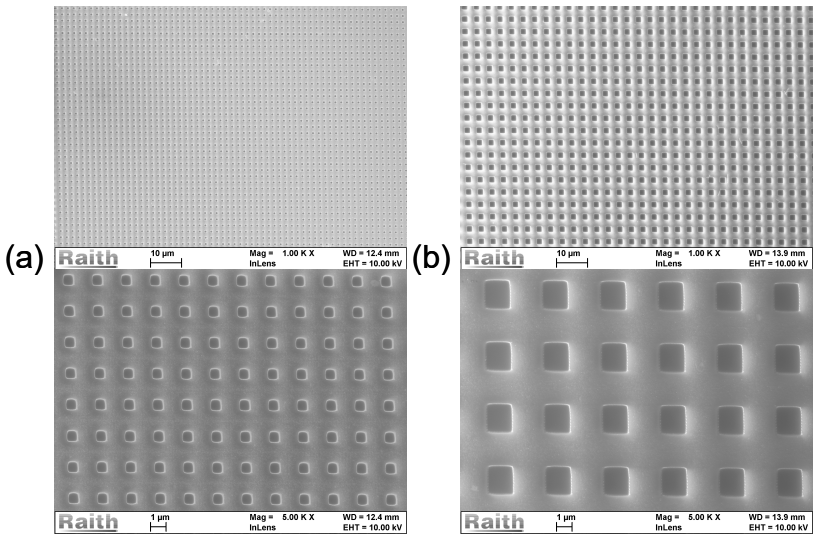

Figure 1. Scanning electronic microscope (SEM) micrographs of electron beam lithography fabricated arrays of (**a**) 1 μm and (**b**) 2 μm square pits at different magnification scales.

Table 1. SF_6 reactive ion etching conditions.

Parameter	Conditions
RF frequency	13.56 MHz
Plasma power density	0.25 W/cm^2
Etching gas	SF_6
Etching gas flow rate	4 sccm
Self-bias voltage	−500 ± 15 V
Chamber pressure	0.12 Pa
Process duration	4 min

2.3. Preparation of the Thiol-Ene Composition, Casting and UV Polymerization

Photopolymerizable thiol-ene composition was prepared as reported previously [26]. A photoinitiator was briefly dissolved in a warm PETMP at 60 °C in an amber glass jar, then the calculated amount of TTT was added, avoiding direct day or artificial light. Components were thoroughly mixed with a spatula. The prepared clear, colorless, viscous mixture was applied on the fabricated micro imprint stamps. Samples were cured simultaneously at the intensities of 1.64 mW/cm^2 (wavelength: 254 nm) and 0.8 mW/cm^2 (wavelength: 365 nm). After that, the cured network was obtained, denoted as PETMP-TTT. The PETMP-TTT films with imprinted microstructures were obtained by gently peeling the film from the micro imprint stamp. The overall film thickness was 100 µm. Afterwards, PETMP-TTT films were cooled down below 0 °C (i.e., programming temperature) and left to stand at room temperature for 5 min prior to further testing. The quenching procedure of the PETMP-TTT film served as a freezing process for the internal strain energy, which is the primary driving force for the shape recovery of the polymeric films. The overall fabrication process of microstructured PETMP-TTT film is shown in Figure 2.

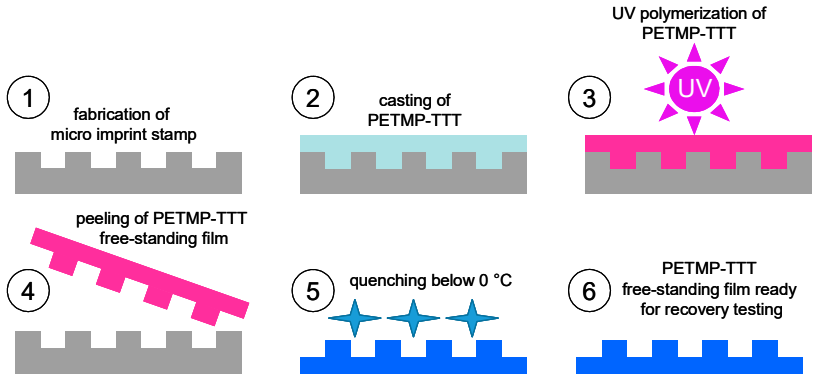

Figure 2. Schematic representation of the microstructured PETMP-TTT film fabrication process from steps (1) to (6).

2.4. Mechanical Deformation and Recovery

Microstructured PETMP-TTT films were deformed by a mechanical press at a pressure of 40 MPa and a temperature of 20 °C for 15 min. The polished steel disk of 6 mm in diameter was used in the mechanical deformation tests. Heat treatment for recovery process of the deformed PETMP-TTT films was performed in an oven at 100 °C (i.e., recovery temperature) for 1 h under an air atmosphere. It is worth mentioning that glass transition temperature (T_g) for the particular thiol-ene composition is 41 ± 1 °C, as reported in our previous work [26]. The glassy transition is the primary mechanism that governs the shape-memory behavior of PETMP-TTT film.

2.5. Characterization

The recovery behavior of deformed PETMP-TTT film was investigated using atomic force microscopy (AFM) and optical microscopy. AFM experiments were carried out at room temperature using a NanoWizardIII atomic force microscope (JPK Instruments, Bruker Nano GmbH, Berlin, Germany), while the data were analyzed using a SurfaceXplorer (Microtestmachines, Gomel, Belarus) and JPKSPM Data Processing software (Version spm-4.3.13, JPK Instruments, Bruker Nano GmbH). The AFM images were collected using a V-shaped silicon cantilever (spring constant of 3 N/m, tip curvature radius of 10.0 nm and cone angle of 20°) operating in contact mode. Digital photographs (B-600MET, OPTIKA Srl, Ponteranica, Italy) were captured (CCD detector) using visible light illumination transmitted from an LED source. Diffraction intensity distribution of the light transmitted through microstructured PETMP-TTT film was observed via illumination with 5 mW green laser (λ = 532 nm).

3. Results and Discussion

Optical microscope image of a boundary separating 2A imprinted and mechanically deformed areas of microstructured PETMP-TTT film is shown in Figure 3. The imprinted film with clearly visible periodic microstructures and a certain waviness of the rear side is seen on the right side of the image. On the left side, part of the deformation made on the film surface by cold pressing of the polished steel disk of 6 mm in diameter is depicted. In this area, periodic micropillars are substantially flattened and are hard to see. Moreover, they are superimposed with the pattern resulting from the surface texture of the steel disk. Large pressing force resulted in a fairly deep deformation. Additionally, the imprinted area is surrounded by the slope with the lateral dimensions of 33–42 µm, which is seen at the middle of the image.

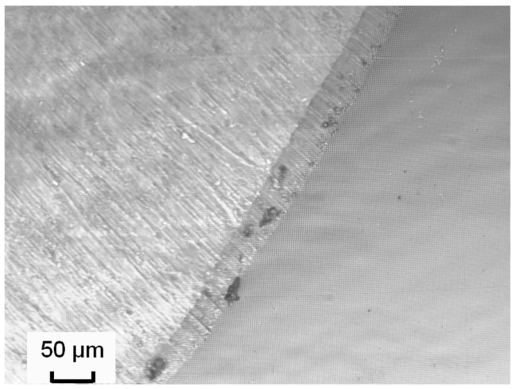

Figure 3. Optical microscope image at 300× magnification of a boundary between 2A imprinted and mechanically deformed areas of the microstructured PETMP-TTT film.

Figure 4 shows AFM 3D topographical images of the PETMP-TTT film surface with 2A and 4B imprinted; it shows deformed and recovered micropillars. The AFM topographical images clearly indicate that the PETMP-TTT film surface microstructures were deformed (Figure 4(a2,b2)) after compression and closely recovered (Figure 4(a3,b3)) to their original shape (Figure 4(a1,b1)) after the heat treatment process.

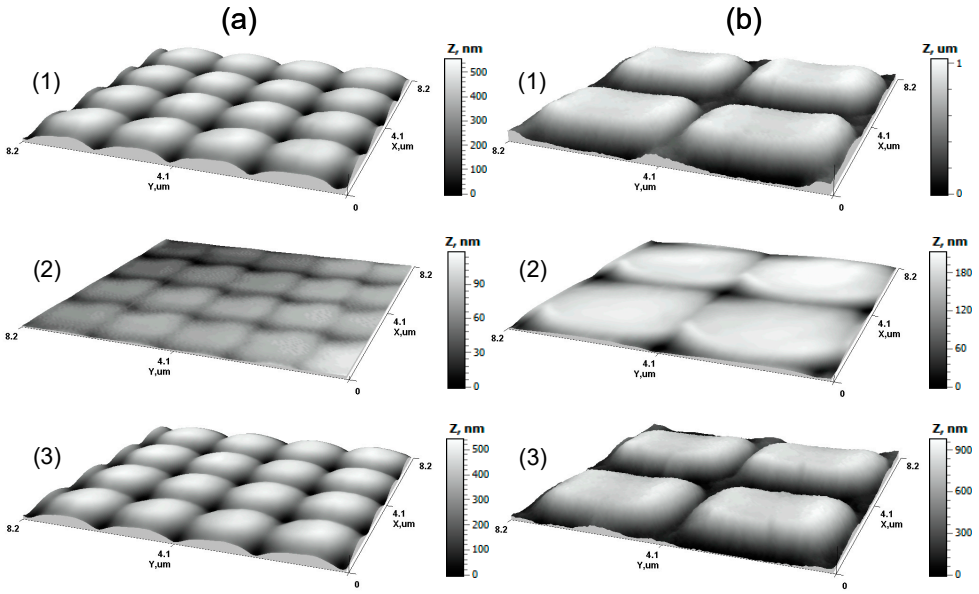

Figure 4. Atomic force microscopy (AFM) 3D topographical images with normalized Z axis in nm: (**a1**) 2A and (**b1**) 4B imprinted micropillars on the PETMP-TTT film surface; (**a2**,**b2**) corresponding micropillars after deformation; (**a3**,**b3**) micropillars after recovery.

Figure 5 shows the AFM height profile images of the 2A and 4B square pits, corresponding to imprinted microstructures on the PETMP-TTT free-standing film surface as well as microstructures after deformation and recovery. Based on AFM, the dimensions of imprinted microstructures in the form of pillars (Figure 5(a2,b2)) were measured and compared with the dimensions of the 2A (Figure 5(a1)) and 4B (Figure 5(b1)) square pits. The AFM height profiles were used for measurements. In all instances, the yields of the pattern transfer into PETMP-TTT films were not worse than 92% ± 2% and 96% ± 2% for 2A and 4B, respectively. The UV-imprinted PETMP-TTT surface micropillars matched closely to the dimensions of the micro imprint stamp square pits. The small differences in dimensions could be attributed to the incomplete filling of the micro imprint stamp square pits, arising from the competition between capillary flow and pressure flow [27]. Nevertheless, these initial profiles of the imprinted microstructures do not affect the mechanical deformation and recovery investigations, therefore 2A and 4B imprinted micropillars were chosen as permanent structures.

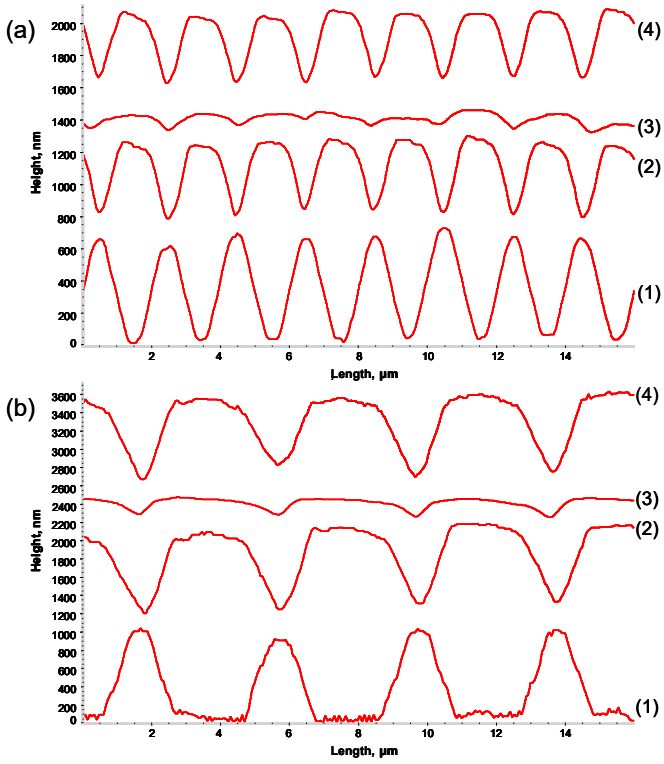

Figure 5. AFM height profile images: (**a1**) 2A and (**b1**) 4B square pits; (**a2**,**b2**) corresponding imprinted micropillars; (**a3**,**b3**) micropillars after deformation; (**a4**,**b4**) micropillars after recovery.

Compression was applied as a mechanical stimulus to deform the microstructured PETMP-TTT polymer films at a pressure of 40 MPa and a temperature of 20 °C for 15 min. The initial height of imprinted 2A (Figure 5(a2)) and 4B (Figure 5(b2)) micropillars was determined to be 495 (±2%) nm and 850 (±2%) nm. The micropillars were deformed by the mechanical press, resulting in the heights of 2A (Figure 4(a3)) and 4B (Figure 5(b3)) being 87 (±2%) nm and 133 (±2%) nm, respectively. After heat treatment of the deformed PETMP-TTT film, the recovery yields for microstructures were found to be not worse than 90% ± 2% and 93% ± 2% for 2A (Figure 5(a4)) and 4B (Figure 5(b4)) with micropillar heights of 451 (±2%) nm and 808 (±2%), respectively. This result is an indication that microstructured PETMP-TTT film exhibits shape-memory effect and is capable of effective surface pattern recovery.

Further quantification of the shape-memory properties of microstructured PETMP-TTT films was performed via analysis of digital photographs and laser diffraction patterns (Figure 6). Very clear diffraction colors can be observed for the imprinted PETMP-TTT films; laser diffraction peaks are very intense and distinct (Figure 6(a1,b1)). After the deformation of PETMP-TTT films, the diffraction colors

almost disappear and the intensity of the laser diffraction peaks decreases significantly (Figure 6(a2,b2)). Heat treatment of the deformed PETMP-TTT films resulted in the recovery of the intense diffraction colors and laser diffraction patterns (Figure 6(a3,b3)). Figure 7 shows normalized diffraction intensity distributions of 2A and 4B microstructured PETMP-TTT films. The latter exhibited 87% ± 2% recovery of the total intensity in the zero, first and second diffraction orders, while 2A resulted in the slightly lower recovery of 83% ± 2%. Alterations in the laser diffraction patterns confirm the shape-memory properties of the PETMP-TTT film and support the results of the AFM analysis.

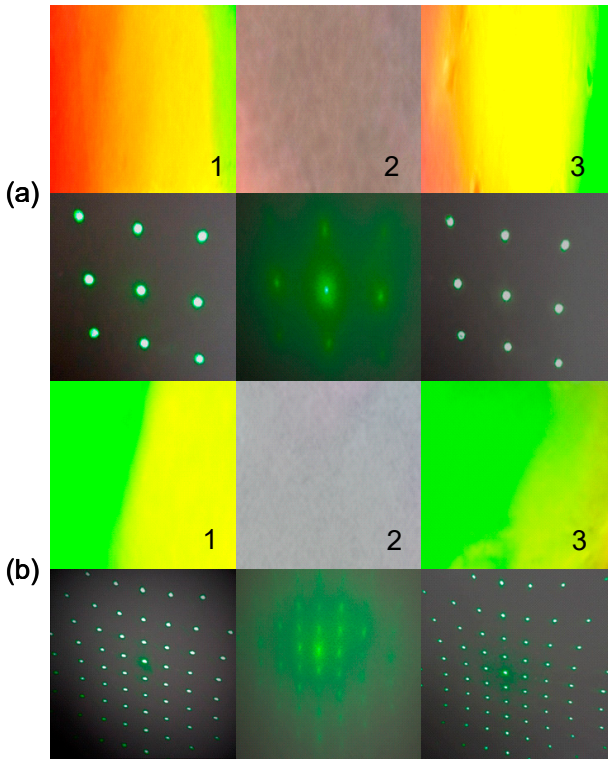

Figure 6. Digital photographs and laser diffraction patterns of the (**a**) 2A and (**b**) 4B microstructured PETMP-TTT films: (1) imprinted, (2) after deformation, (3) after recovery.

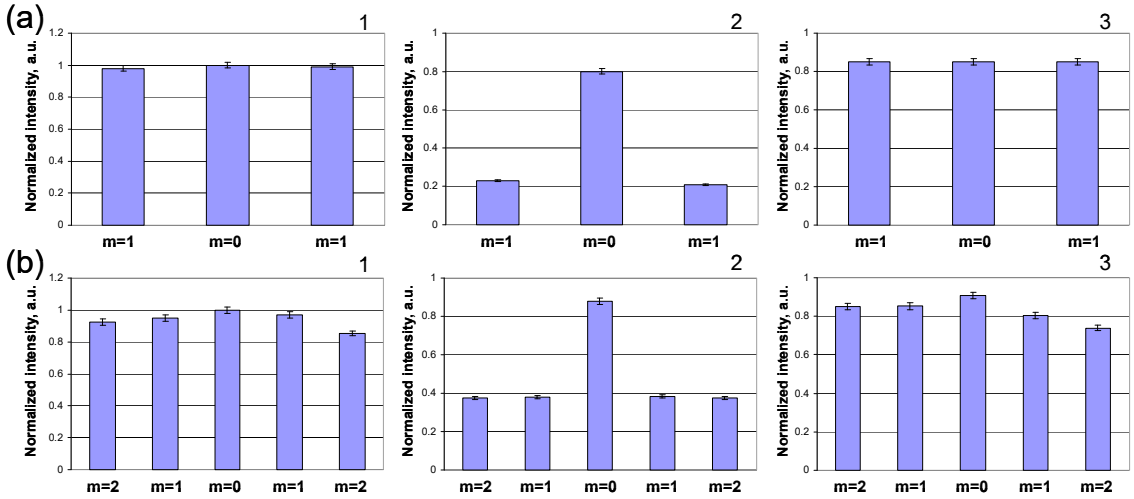

Figure 7. Normalized diffraction intensity distribution of the (**a**) 2A and (**b**) 4B microstructured PETMP-TTT films: (1) imprinted, (2) after deformation, (3) after recovery.

Herein, it was demonstrated that surface microstructurization coupled with a shape-memory polymer generates reversibly tunable surface properties, e.g., the recovery of the laser diffraction

patterns. Microstructured thermoset thiol-ene films exhibiting thermo-responsive shape-memory properties could find application in optical security devices or sustainable superhydrophobic coatings for advanced manufacturing. They can be used to regulate flow in mili/micro/nano channels for medical diagnostics and biosensors.

4. Conclusions

Microstructured PETMP-TTT films were fabricated via casting and UV polymerization on electron beam lithography-fabricated arrays of 1 and 2 μm square pits. Compression was applied as a mechanical stimulus to deform the microstructured PETMP-TTT polymer films. Recovery behavior was investigated via AFM analysis of digital photographs and laser diffraction patterns. It was found that heat treatment of the deformed PETMP-TTT films at 100 °C for 1 h resulted in recovery yields that were not worse than 90% ± 2% and 93% ± 2% for 2A and 4B imprinted micropillars, respectively. Additionally, the shape-memory properties of the microstructured films were quantified by the recovery of intense diffraction colors and laser diffraction patterns. The 4B microstructured PETMP-TTT film exhibited 87% ± 2% recovery of the total intensity in the zero, first and second diffraction orders, while 2A exhibited a slightly lower recovery of 83% ± 2%. The laser diffraction patterns were shown to be suitable for the rapid evaluation of recovered shape-memory profiles. It was demonstrated that surface microstructurization coupled with a shape-memory polymer generates reversibly tunable surface properties, which could find application in optical security devices, sustainable superhydrophobic coatings, etc.

Author Contributions: Conceptualization, V.G.; Methodology, A.L., V.G. and D.J.; Validation, A.L., V.G. and D.J.; Formal Analysis, A.L., V.G. and D.J.; Investigation, A.L., V.G. and D.J.; Resources, A.L.; Writing—Original Draft Preparation, A.L., V.G. and D.J.; Writing—Review and Editing, A.L., V.G. and D.J.; Visualization, A.L., V.G. and D.J.; Supervision, A.L.; Project Administration, A.L.; Funding Acquisition, A.L.

Funding: This research was (and is) funded by the European Social Fund under the No 09.3.3-LMT-K-712-01 "Improvement of researchers' qualification by implementing world-class R&D projects" measure. Grant No. 09.3.3-LMT-K-712-01-0074.

Acknowledgments: Special thanks go to Asta Guobienė and Valentinas Baltrušaitis from Kaunas University of Technology.

Conflicts of Interest: The authors declare no conflict of interest.

References

1. Wen, C.; Yu, X.; Zeng, W.; Zhao, S.; Wang, L.; Wan, G.; Huang, S.; Grover, H.; Chen, Z. Mechanical behaviors and biomedical applications of shape memory materials: A review. *AIMS Mater. Sci.* **2018**, *5*, 559–590. [CrossRef]
2. Pilate, F.; Toncheva, A.; Dubois, P.; Raquez, J.-M. Shape-memory polymers for multiple applications in the materials world. *Eur. Polym. J.* **2016**, *80*, 268–294. [CrossRef]
3. Kalita, H. *Shape Memory Polymers: Theory and Application*; Walter de Gruyter GmbH & Co KG: Berlin, Germany, 2018.
4. Hager, M.D.; Bode, S.; Weber, C.; Schubert, U.S. Shape memory polymers: Past, present and future developments. *Prog. Polym. Sci.* **2015**, *49*, 3–33. [CrossRef]
5. Ramdas, M.R.; Kumar, K.S.; Nair, C.R. Click polymerizations: Encouraging route for shape memory polymers. *Mater. Lett.* **2016**, *172*, 216–221. [CrossRef]
6. Jiang, Z.-C.; Xiao, Y.-Y.; Kang, Y.; Pan, M.; Li, B.-J.; Zhang, S. Shape memory polymers based on supramolecular interactions. *ACS Appl. Mater. Interfaces* **2017**, *9*, 20276–20293. [CrossRef]
7. Mu, T.; Liu, L.; Lan, X.; Liu, Y.; Leng, J. Shape memory polymers for composites. *Compos. Sci. Technol.* **2018**, *160*, 169–198. [CrossRef]
8. Wang, K.; Strandman, S.; Zhu, X. A mini review: Shape memory polymers for biomedical applications. *Front. Chem. Sci. Eng.* **2017**, *11*, 143–153. [CrossRef]
9. Xie, F.; Huang, L.; Leng, J.; Liu, Y. Thermoset shape memory polymers and their composites. *J. Intell. Mater. Syst. Struct.* **2016**, *27*, 2433–2455. [CrossRef]

10. Lee, W.L.; Low, H.Y. Geometry-and length scale-dependent deformation and recovery on micro-and nanopatterned shape memory polymer surfaces. *Sci. Rep.* **2016**, *6*, 23686. [CrossRef] [PubMed]
11. Liu, N.; Xie, Q.; Huang, W.; Phee, S.; Guo, N. Formation of micro protrusion arrays atop shape memory polymer. *J. Micromech. Microeng.* **2008**, *18*, 027001. [CrossRef]
12. Peng, H.-G.; Kong, Y.P.; Yee, A.F. Relaxation kinetics of nanostructures on polymer surface: Effect of stress, chain mobility, and spatial confinement. *Macromolecules* **2010**, *43*, 409–417. [CrossRef]
13. Chen, C.-M.; Yang, S. Directed water shedding on high-aspect-ratio shape memory polymer micropillar arrays. *Adv. Mater.* **2014**, *26*, 1283–1288. [CrossRef] [PubMed]
14. Wu, Z.L.; Wei, R.; Buguin, A.; Taulemesse, J.-M.; Le Moigne, N.; Bergeret, A.; Wang, X.; Keller, P. Stimuli-responsive topological change of microstructured surfaces and the resultant variations of wetting properties. *ACS Appl. Mater. Interfaces* **2013**, *5*, 7485–7491. [CrossRef] [PubMed]
15. Xu, H.; Yu, C.; Wang, S.; Malyarchuk, V.; Xie, T.; Rogers, J.A. Deformable, programmable, and shape-memorizing micro-optics. *Adv. Funct. Mater.* **2013**, *23*, 3299–3306. [CrossRef]
16. Lowe, A.B. Thiol-ene "click" reactions and recent applications in polymer and materials synthesis. *Polym. Chem.* **2010**, *1*, 17–36. [CrossRef]
17. Nair, D.P.; Cramer, N.B.; Scott, T.F.; Bowman, C.N.; Shandas, R. Photopolymerized thiol-ene systems as shape memory polymers. *Polymer* **2010**, *51*, 4383–4389. [CrossRef]
18. Hoyle, C.E.; Lowe, A.B.; Bowman, C.N. Thiol-click chemistry: A multifaceted toolbox for small molecule and polymer synthesis. *Chem. Soc. Rev.* **2010**, *39*, 1355–1387. [CrossRef] [PubMed]
19. Fouassier, J.-P.; Rabek, J.F. *Radiation Curing in Polymer Science and Technology: Practical Aspects and Applications*; Springer Science & Business Media: Berlin, Germany, 1993; Volume 4.
20. Morgan, C.; Magnotta, F.; Ketley, A. Thiol/ene photocurable polymers. *J. Polym. Sci. Part A Polym. Chem.* **1977**, *15*, 627–645. [CrossRef]
21. Hoyle, C.E.; Lee, T.Y.; Roper, T. Thiol–enes: Chemistry of the past with promise for the future. *J. Polym. Sci. Polym. Chem.* **2004**, *42*, 5301–5338. [CrossRef]
22. Cramer, N.B.; Couch, C.L.; Schreck, K.M.; Carioscia, J.A.; Boulden, J.E.; Stansbury, J.W.; Bowman, C.N. Investigation of thiol-ene and thiol-ene–methacrylate based resins as dental restorative materials. *Dent. Mater.* **2010**, *26*, 21–28. [CrossRef] [PubMed]
23. Reddy, S.K.; Cramer, N.B.; Bowman, C.N. Thiol-vinyl mechanisms. 1. Termination and propagation kinetics in thiol-ene photopolymerizations. *Macromolecules* **2006**, *39*, 3673–3680. [CrossRef]
24. Tähkä, S.M.; Bonabi, A.; Nordberg, M.-E.; Kanerva, M.; Jokinen, V.P.; Sikanen, T.M. Thiol-ene microfluidic devices for microchip electrophoresis: Effects of curing conditions and monomer composition on surface properties. *J. Chromatogr. A* **2015**, *1426*, 233–240. [CrossRef] [PubMed]
25. White, T.J.; Natarajan, L.V.; Tondiglia, V.P.; Lloyd, P.F.; Bunning, T.J.; Guymon, C.A. Holographic polymer dispersed liquid crystals (HPDLCs) containing triallyl isocyanurate monomer. *Polymer* **2007**, *48*, 5979–5987. [CrossRef]
26. Lazauskas, A.; Jucius, D.; Baltrušaitis, V.; Gudaitis, R.; Prosyčevas, I.; Abakevičienė, B.; Guobienė, A.; Andrulevičius, M.; Grigaliūnas, V. Shape-memory assisted scratch-healing of transparent thiol-ene coatings. *Materials* **2019**, *12*, 482. [CrossRef] [PubMed]
27. Rowland, H.D.; Sun, A.C.; Schunk, P.R.; King, W.P. Impact of polymer film thickness and cavity size on polymer flow during embossing: Toward process design rules for nanoimprint lithography. *J. Micromech. Microeng.* **2005**, *15*, 2414. [CrossRef]